CERN 84-01
8 February 1984

ORGANISATION EUROPÉENNE POUR LA RECHERCHE NUCLÉAIRE
CERN EUROPEAN ORGANIZATION FOR NUCLEAR RESEARCH

COMPUTER PROGRAMS IN ACCELERATOR PHYSICS

Eberhard Keil

Lectures given at the
1982 SLAC Summer School
on Physics of High-Energy Particle Accelerators
and in the Academic Training Programme of CERN 1982–1983

GENEVA
1984

CERN – Service d'Information scientifique – RD/625 – 3000 — Février 1984

ABSTRACT

Three areas of accelerator physics are discussed in which computer programs have been applied with much success: i) single-particle beam dynamics in circular machines, i.e. the design and matching of machine lattices; ii) computations of electromagnetic fields in RF cavities and similar objects, useful for the design of RF cavities and for the calculation of wake fields; iii) simulation of betatron and synchrotron oscillations in a machine with non-linear elements, e.g. sextupoles, and of bunch lengthening due to longitudinal wake fields.

CONTENTS

INTRODUCTION

This series of three lectures covers three distinct areas in accelerator physics to which computer programs have been applied with much success. These are:

i) Lattice optimization

This covers the beam dynamics in circular machines consisting of drift spaces, bending magnets, and focusing elements. Space-charge effects, i.e. the interaction between the particles in the beam, and between the beam and its surroundings, are neglected. Also included is a simple procedure for estimating the parameters of e^+e^- storage rings.

ii) Electromagnetic fields

Time-varying electromagnetic fields play an important role in accelerator physics, in particular in the design of RF accelerating systems and in the theory of instabilities due to the interaction between the beam and its surroundings.

iii) Simulation

Several problems in accelerator physics which are not amenable to analytic solution can be studied by computer simulation. Two examples are discussed, the first involving betatron oscillations in a machine lattice including sextupoles, and the second involving synchrotron oscillations in the presence of wake fields.

In the framework of these lectures, it is impossible to cover all aspects of accelerator physics and all computer programs (not even those which I consider useful) in adequate detail. Hence, only a few examples are discussed at length. However, other useful programs are mentioned briefly, including references to where documentation can be found or obtained.

1. COMPUTER PROGRAMS FOR LATTICE OPTIMIZATION

1.1 Introduction

1.1.1 Purpose

This lecture is intended to serve several purposes, namely

i) to present the accelerator physics underlying a lattice optimization,

ii) to show a broad outline of how a lattice is optimized, and

iii) to give an overview of the computer programs involved.

All the accelerator physics which will be used here is described in the existing literature; references [1] to [4] contain useful material. No derivations are given; however, important and relevant results will be stated and discussed briefly.

Many different computer programs (written by many different people) can be used for optimizing a lattice and computing its properties in great detail. A (not necessarily exhaustive) list of the more popular programs will be given, together with a description of what they can do and how they do it.

1.1.2 Lattice/Optimization definition

The term "lattice" is used for an arrangement of field-free straight sections, dipoles, and quadrupoles in a closed loop of roughly circular shape. In the discussion here, the functions of bending and focusing are separated. The dipoles keep the particles on a nearly circular orbit, the equilibrium orbit, whilst the quadrupoles focus the particles according to the principle of alternating-gradient focusing. Other magnetic elements, e.g. sextupoles, solenoids, orbit correction magnets, although necessary for the final design of any large accelerator, are beyond the scope of this lecture.

"Lattice optimization" is the process of discovering a set of lattice parameters, e.g. the length of the dipoles, quadrupoles, and the straight sections, their aperture, the field strength for the dipoles, and the gradient of the quadrupoles. In addition, the most important parameters of the RF accelerating system have to be determined, e.g. frequency, total length, and circumferential voltage, and also an estimate of the expected performance, e.g. the circulating current and luminosity.

The arguments used in the lattice optimization are based upon:

i) the physics of particle beams in a circular machine;

ii) the design and fabrication of machine components; and

iii) the cost of these components.

The aim of this process is to arrive at the cheapest machine which reaches the specified performance whilst obeying the laws of physics and the principles of good engineering.

1.1.3 e^+e^- versus pp or $p\bar{p}$

This lecture will be restricted to the optimization of e^+e^- storage ring lattices. Storage ring lattices contain more physics than accelerator lattices because more beam parameters must be controlled. In an accelerator, usually only maximum energy and intensity are specified. Synchrotron radiation makes e^+e^- storage ring lattices quite interesting because the balance between quantum excitation and radiation damping leads to a relation between the *beam* and *lattice* parameters which is *exploited* in the optimization. In a pp or $p\bar{p}$ storage ring, Liouville's theorem holds. Hence, the *beam* parameters are determined by the *injector*, beam manipulations in the storage ring proper, and the energy.

1.1.4 Outline of procedure

The optimization procedure is based upon a simplified model of the e^+e^- storage ring. The arrangement of magnets and straight sections can be divided into superperiods which are repeated 2k times around the circumference. There are k bunches in each of the two counter-rotating beams which collide in 2k equidistant crossing points. For further simplification, each superperiod is divided into two halves which are mirror images of each other. One such half superperiod is shown in Fig. 1.1. It starts with a crossing point at the left and contains the following building blocks:

i) the low-β insertion with straight sections and quadrupoles;
ii) the RF section with straight sections, RF accelerating cavities, and quadrupoles;
iii) the dispersion suppressor with straight sections, dipoles, and quadrupoles; and
iv) standard lattice cells with straight sections, dipoles, and quadrupoles.

The procedure can be split into two stages. The parameters of the standard lattice cells are determined in the first stage and all the other parameters in the second stage. In order to split the problem in this way, it is assumed that the beam emittance in the whole storage ring is determined only by the parameters of the standard lattice cell. Since the current design practice demands vanishing dispersion in the low-β insertion and the RF section, this assumption is justified. The small effect of the dispersion suppressor on the beam emittance is neglected for the first stage.

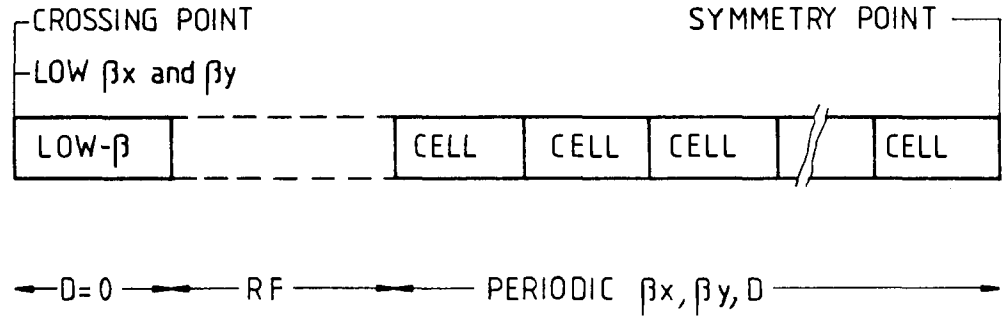

Fig. 1.1 Simplified layout of half a superperiod in the e^+e^- storage ring model.

1.2 Some basic machine physics [5]

1.2.1 Size scaling

The main argument for choosing the size of a machine, i.e. the bending radius ρ and the total length of RF cavities L_c, comes from minimizing its cost. The two parameters above are related by the synchrotron radiation loss $U_s \sim E^4/\rho$. An optimum RF system has a given voltage gradient, and hence its length $L_c \approx U_s$. If ρ is small, savings occur in the cost of the tunnel, magnets, vacuum chambers, etc.; however, the cost for RF

cavities and power sources is high. If ρ is large, the opposite holds. An approximate cost minimum is reached when all lengths scale with the energy E in the same way, like E^2 [6]:

$$\rho \sim R \sim C/2\pi \sim L_c \sim E^2 . \tag{1.1}$$

Here, R and C are the average radius of the arcs and the circumference. The following inequalities will be useful later:

$$\rho < R < C/2\pi , \tag{1.2}$$

$$2\pi R + L_c < C . \tag{1.3}$$

1.2.2 Luminosity

Consider bunches of electrons and positrons travelling in opposite directions along the s-axis in the coordinate system shown in Fig. 1.2. The density distributions are Gaussian with standard deviations σ_x, σ_y, σ_s along the three coordinate axes. The performance of a storage ring is described by its luminosity L, given by

$$L = \frac{N^2 f}{4\pi k \sigma_x \sigma_y} . \tag{1.4}$$

Here, N is the total number of particles, k the number of bunches in each beam, and f the revolution frequency. The event rate for any process is simply the product of the luminosity and the cross-section. In order to maximize the luminosity, N should be large, and σ_x and σ_y small.

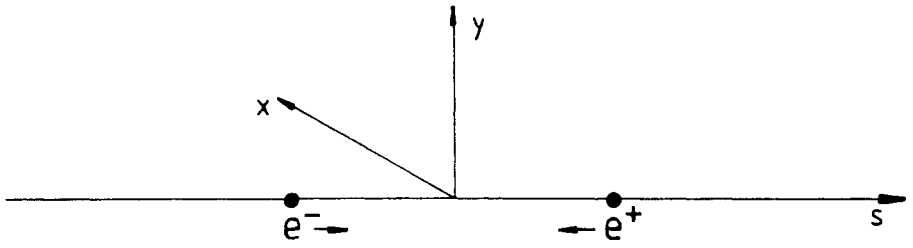

Fig. 1.2 Coordinate system describing beam–beam collisions.

1.2.3 Beam-beam tune shift

The particles in the e^+ (e^-) bunch are subjected to the electromagnetic field carried by the e^- (e^+) bunch travelling in the opposite direction. The most important effect is a transverse deflection which vanishes along the s-axis because of symmetry. Since the bunches travel in opposite directions, the electric and magnetic fields *add*, each contributing about half the total effect for $\gamma \gg 1$. Since the bunch charges are of opposite sign, the force is attractive. The lowest-order effect is a linear focusing effect, almost like a quadrupole (except focusing in both planes), which increases the tunes Q_x and Q_y of the machine by the linear beam-beam tune shifts ΔQ_x and ΔQ_y :

$$\Delta Q_x = \frac{N r_e \beta_x}{2\pi k \gamma (\sigma_x + \sigma_y)\sigma_x} , \tag{1.5}$$

$$\Delta Q_y = \frac{N r_e \beta_y}{2\pi k \gamma (\sigma_x + \sigma_y)\sigma_y} , \tag{1.6}$$

where r_e is the classical electron radius, β_x and β_y are the horizontal and vertical amplitude functions at the interaction points, respectively, and γ is the usual relativistic factor.

$$D = \frac{L_p \phi}{4} \left(1 \pm \frac{1}{2} \sin \frac{\mu}{2}\right) \Big/ \sin^2 \frac{\mu}{2} \quad . \tag{1.20}$$

Here, β and D are taken at the quadrupoles, the upper (lower) sign applies to the focusing (defocusing) quadrupole, and the edge focusing of the bending magnets is neglected, i.e. $\phi \ll 1$.

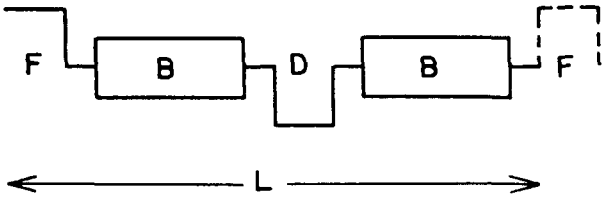

a) FODO Lattice

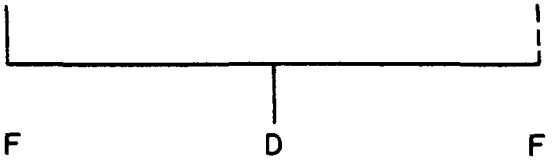

b) Thin-lens FODO lattice

Fig. 1.3 Schematic layout of a FODO lattice cell with quadrupoles D and F and bending magnets B. The thin-lens equivalent is also shown.

1.3.2 Beam size and aperture

There are two contributions to the horizontal beam size in the standard cells: betatron oscillations and energy spread. Adding them quadratically yields the following r.m.s. beam radius:

$$\sigma_x^2 = E_x \beta_x + (D\sigma_e)^2 \quad . \tag{1.21}$$

The radial half-aperture A_x must be a certain multiple F_x of σ_x, and it is common to make an allowance C_x for horizontal closed-orbit distortions, hence

$$A_x = F_x \sigma_x + C_x \quad . \tag{1.22}$$

The factor $F_x \gg 1$ is obtained by imposing a lower limit on the beam lifetime with respect to particle losses at the edge of the aperture. This can be done by considering the probability that a particle with amplitude $F_x\sigma_x$ increases its amplitude even further, similar to the quantum lifetime calculation for fixing RF bucket parameters. The result is $F_x = 6...7$, which is usually rounded up to $F_x = 10$.

The arguments leading to the vertical half-aperture A_y are not so straightforward. In an ideal machine with $D_y = 0$, the vertical quantum excitation and hence the vertical emittance are very small, because the photon emission angle is of the order of $1/\gamma$. In a real machine with alignment errors the vertical dispersion D_y does not vanish, but since $\bar{D}_y$ is usually less than $\bar{D}_x$, the same holds for the beam sizes. In order to have equal beam-beam tune shifts in the two planes, the beam sizes at the crossing points must be in the ratio of the β's there. This implies that also:

$$E_y/E_x = \beta_y/\beta_x \quad . \tag{1.23}$$

The vertical emittance used in most existing machines is obtained by requiring that an emittance exchange on a coupling resonance should not cause beam loss. Excluding the case of very different damping partition numbers J_x and J_y this implies, from equipartition of transverse energy,

$$E_{xc} \approx E_{yc} = \frac{1}{2} E_x \ . \tag{1.24}$$

The vertical half-aperture then becomes

$$A_y = F_y \left(\frac{1}{2} E_x \beta_y \right)^{1/2} + C_y \ . \tag{1.25}$$

The arguments for putting $F_y \approx 10$ are the same as for F_x. It should be noted in passing that the beam-beam limit ΔQ increases with the vertical aperture.

1.3.3 DESIGN

All the considerations presented so far have been incorporated in a computer program, DESIGN [9]. A typical output is shown in Fig. 1.4. Input quantities are marked. DESIGN also computes the parameters of the RF system, including quantum lifetime and transient beam loading.

```
STORAGE RING DESIGN PROGRAM   VERSION 3                                  27/02/83
----------------------------------------

PG ,  BXS  , LPD          HAVE BEEN READ IN AS DATA

BEAM PARAMETERS AND LUMINOSITY
------------------------------

ENERGY =    75.0000  GEV              DQX   =      .0600                DQY     =      .0600
U0     =   789.5431  MEV/REV          TAUE  =     9.6976  MSEC         COUPLING=      .2500
SIGE   = .1079E-02   DE/E             SIGX* =      .3527  MM           SIGY*   =      .0220  MM
L      = .9930E+32   1/CM**2/SEC      N     = .6488E+13   PER BEAM     IB      =     2.5456  MA/BUNCH
K      =      4      BUNCHES


LATTICE PARAMETERS
------------------

RHO    = 3545.0000  M                R     =  4030.0000  M            C/2PI   = 4871.0000  M
MU/2PI =     .1544  1/CELL           F     =     9.7954  KHZ          Q       =   49.4763
LP     =   79.0000  M                BETMAX=   140.4263  M            BETMIN  =   51.1307  M
SIGXMAX=    4.1713  MM               BETX* =     1.6000  M
SIGYMAX=     .8515  MM               BETY* =      .1000  M
FX     =   10.0000                   CX    =    20.0000  MM           AX      =   61.7134  MM
FY     =   10.0000                   CY    =    10.0000  MM           AY      =   34.0832  MM


RF RELATED PARAMETERS
---------------------

H      =      36076                  VRF   =  1285.7863  MV           FRF     =  353.3793  MHZ
GAMMA  =      .7091                  QS    =      .1532                P       = .8039E+01  MW
SIGB   = .1079E-01   RF BUCKET       SIGZ  =    11.5980  MM           TAUQ    =   24.0000  HOURS
SHUNT  = .4000E+02   MEGOHM/M        LC    = .1086E+04   M            PG      = .5920E+02  MW
ZHM    = .1200E+05   MEGOHM          TFILL = .5650E-01   MSEC
BETARF = .1397E+01                   PSI   = -.8874E+01  DEGREES

BUCKET =    10.000
```

Fig. 1.4 Example of output from the DESIGN program.

1.4 Lattice design with optics programs

1.4.1 Starting point: Design results and trivialities

We are now almost ready to continue the lattice design with optics programs, using as a starting point the results obtained with the DESIGN procedure. However, a few things still need be done to the machine, shown schematically in Fig. 1.5. These are listed below.

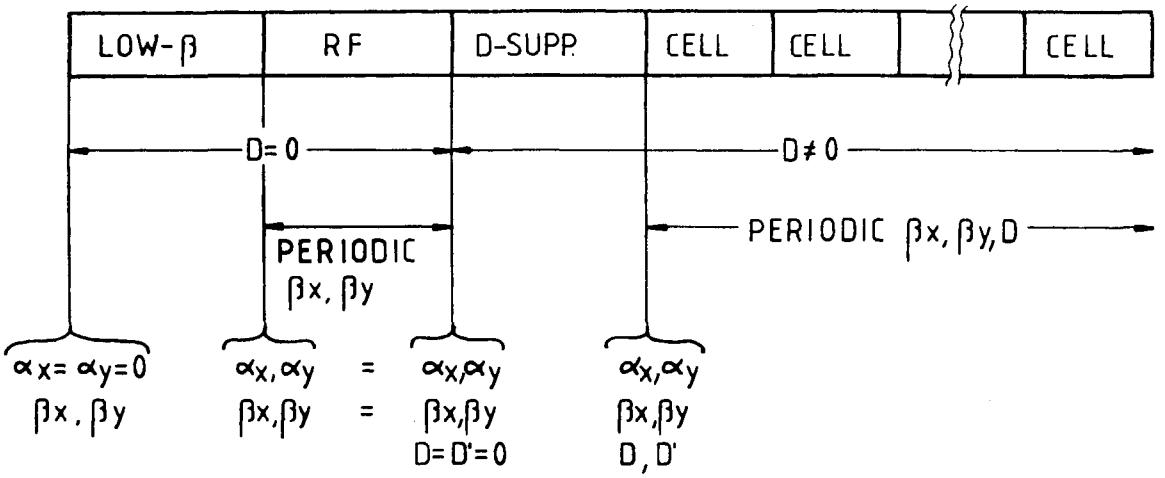

Fig. 1.5 Schematic layout of half a superperiod in the e^+e^- storage ring model. The places where matching conditions are imposed are also indicated.

- Fix the length of the cell quadrupoles, ℓ_Q, using the strength (1.18), aperture radius, A_Q, maximum operating energy and pole-tip field, B_Q, related by

$$\frac{B_Q \ell_Q}{A_Q B\rho} = \frac{4}{L_p} \sin \frac{\mu}{2} . \tag{1.26}$$

- Fix the length of cell sextupoles and orbit correction magnets, which are outside the scope of this lecture.
- Determine a cell layout which houses all these magnets and the dipoles, and leaves adequate space for coil overhangs, bellows, beam-position monitors, etc.
- Adopt a design for a dispersion suppressor. All dispersion suppressor designs have a natural dispersion which is smaller than that of the lattice. A forced oscillation of about half a wavelength reduces the dispersion from the lattice value to zero. The reduction of the dispersion is achieved by increasing the focusing, or by reducing the bending, or by a combination of both [see Eq. (1.20)].
- Design the lattice of the RF section, which includes fixing the quadrupole length, providing the space for the RF cavities and other equipment, and making the cell length an integral multiple of an RF wavelength.
- Design the low-β insertion, observing constraints on the free space ℓ_x from the crossing point to the nearest quadrupole and constraints on the quadrupole length.
- Get the correct over-all machine geometry, e.g. circumference, total bending angle 2π.

Should the over-all machine parameters, e.g. R and ρ, change significantly in this process, a further iteration through the DESIGN procedure might be in order.

1.4.2 Conditions and variables

Since the machine geometry is fixed, apart from the position of a few quadrupoles in the low-β insertion, the matching conditions must mostly be satisfied by varying the quadrupole gradients. The conditions to be satisfied are also shown in Fig. 1.5.

1) In the cells, the quadrupole gradients must be determined such that the desired phase advances μ_x and μ_y are obtained. Then, also β_x, β_y, D, and D′ are known for all positions in the cell.

2) In the RF section, the quadrupole gradients must also be determined.

3) The quadrupole gradients in the dispersion suppressor must be determined such that the correct values of β_x, β_y, α_x, α_y, D, and D′ are obtained at the two ends. This implies six conditions and hence at least six variables.

4) The quadrupole gradients in the low-β insertion must be found such that the conditions on β_x, β_y, α_x, and α_y, are satisfied at the two ends. This implies four conditions and hence at least four variables.

5) In order to obtain the correct machine tunes, the total phase advances, through the low-β insertion, the RF section, and the dispersion suppressor, must also be constrained.

All these conditions can be formulated as one single matching operation, starting at the borderline between dispersion suppressor and cells with known values of β_x, β_y, α_x, α_y, D, and D′, and imposing the following conditions: i) $D = D' = 0$ at the limit between RF section and dispersion suppressor; ii) equal values of β_x, β_y, α_x, and α_y at either end of the RF section; iii) fixed values of β_x and β_y, and $\alpha_x = \alpha_y = 0$ at the crossing point; and iv) phase advances from the crossing point to the beginning of the cells. In LEP, fourteen variable quadrupole gradients are used, six each in the low-β insertion and in the dispersion suppressor, and two in the RF section. This is two more than the number of conditions.

1.4.3 Computer programs

A list of general-purpose lattice programs is shown in Table 1.1. All these programs perform the following functions:

i) Read a sequence of elements, a beam line. Some of them have a very compact notation by nesting, repeating, and reflecting beam lines.

ii) Read properties of the elements, e.g. their type (drift space, dipole, quadrupole, sextupole, etc.), their length, their "strength" (bending field or angle, gradient, etc.).

iii) Perform the following calculations on a beam line relevant for lattice matching:
- find the periodic solution for β_x, β_y, α_x, α_y, D_x, D_x', D_y, D_y', and compute phases μ_x and μ_y;
- track the functions β_x, β_y, α_x, α_y, D_x, D_x', D_y, D_y', μ_x, μ_y through a beam line, starting with given initial values of these functions.

iv) Vary specified parameters of elements of the beam line (length, position, strength) such that a specified selection of α_x, α_y, β_x, β_y, D_x, D_x', D_y, D_y', μ_x, μ_y takes prescribed values at specified places along the beam line. These conditions may be imposed on either the periodic or the initial-value problem. Specific examples of such matching conditions were shown earlier.

Table 1.1
General-purpose optics programs

Name	Ref.	Contact	Address
MAGIC	10	M.J. Lee	SLAC
SYNCH	11	A.A. Garren	LBL
TRANSPORT*)	12	K.L. Brown	SLAC
		D. Carey	Fermilab
		F.C. Iselin	CERN
AGS	13	E. Keil	CERN
MAD	14	F.C. Iselin	CERN

*) Note that TRANSPORT now allows constraints on β, α, D, D′, but not on phases. Refer to Ref. [15].

1.4.4 Numerical techniques

Standard numerical techniques are used to solve the matching equations, which form a set of n non-linear equations in $m \geq n$ unknowns x_i:

$$0 = f_i(x_1, \ldots, x_m) , \quad i = 1, \ldots, n . \tag{1.27}$$

MAGIC and TRANSPORT use non-linear equation solvers. AGS and SYNCH construct a mismatch function which is minimized using one of the methods available in the general-purpose minimization package MINUIT [16]. In AGS the function is, with weights w_i chosen by the user,

$$F = \prod_{i=1}^{n} (1 + f_i^2 w_i^2) - 1 \ . \tag{1.28}$$

1.4.5 Pitfalls

Problems may arise when the programs do not find a solution which both satisfies the matching equations and does not have unnecessary peaks and dips in the β-functions and/or dispersion. This failure may be due to numerical difficulties or physical conditions impossible to satisfy. Here are some hints on how these difficulties can be overcome.

i) Start with good guesses for the variables, e.g. calculating quadrupole gradients from thin-lens formulae [Eq. (1.18) for lattice cells]. MAGIC tries to find a solution in two steps: first with thin lenses, and then with thick lenses.

ii) Avoid problems that have no solution, e.g. a dispersion suppressor without bending magnets.

iii) Since zero-finding and minimization in many variables is notoriously difficult, split a problem into several smaller ones. The problem shown in Fig. 1.5 can be divided as follows:
   - match dispersion suppressor to fixed RF section;

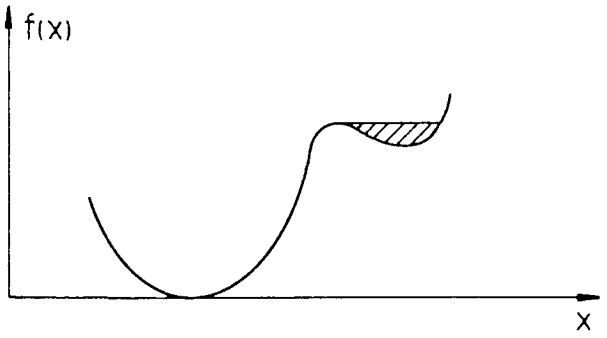

Fig. 1.6 One-dimensional example of a mountain lake.

Table 1.2
Further beam-optics programs

Name	Ref.	Contact	Address	Application
TURTLE	17	K.L. Brown F.C. Iselin	SLAC CERN	Track particles through beam line
PATRICIA	18	H. Wiedemann	SLAC	Optics and electron-beam parameters, chromatic effects, tracking
PETROS	19	J. Kewisch	DESY	Simulate alignment errors; compute and correct closed orbit; compute beam parameters
ALIGN	20	E. Close	LBL	Simulate alignment errors; compute and correct closed orbit
HARMON	21	M. Donald	SLAC	Compute many sextupole effects; adjust sextupole strengths

- match low-β insertion to the same RF section;
- repeat the above steps with different quadrupole gradients in the RF section;
- use results as starting values for full match.

iv) Changing weights such that the program knows what conditions are most important may change the shape of the fit function F such that "mountain lakes" are avoided. A one-dimensional example is shown in Fig. 1.6.

1.5 Other beam optics programs

The matching programs shown in Table 1.1 calculate other things apart from those described so far. In addition, there are several other programs which use the results of a lattice program to calculate more things. These programs are listed in Table 1.2.

2. PROGRAMS FOR ELECTROMAGNETIC FIELD COMPUTATIONS

The calculation of electromagnetic fields by computer programs is useful for accelerator physics in two distinct areas: the engineering of RF accelerating cavities, and the study of the interaction between intense circulating beams and RF cavities.

In the first area — RF cavity engineering — computer programs permit accurate calculations of the resonant frequencies and of the shunt impedance for a few modes including that driven by the RF transmitter. The shape of the cavity can then be modified by hand between computer runs to obtain the desired resonant frequency, and to maximize the shunt impedance per unit length, Z, which appears in the relation between the accelerating gradient, E, and the RF power per unit length, P, required:

$$E^2 = PZ \ . \tag{2.1}$$

This optimization by computer is much faster than building models of RF cavities for measurement. This is the domain of finite-element programs.

In the second area — the interaction between beams and RF cavities — different requirements arise. The electromagnetic fields are not the final aim, but rather essential ingredients for a subsequent investigation of beam stability against all sorts of collective phenomena. The results of the field computation are usually expressed in terms of a complex impedance $Z(\omega)$ as a function of frequency, or as a wake field W(t) as a function of time. One quantity is the Fourier transform of the other. In this application of electromagnetic field computations a wide frequency range should be covered. In the interest of speed, some simplifications of the cavity geometry are necessary. This is the domain of field-matching programs.

For the sake of brevity, the presentation here is limited to RF cavities which are cylindrically symmetric, i.e. their shape is fully described by a simple curve in (r,z)-space as shown in Fig. 2.1. This is not a serious restriction in practice, because RF cavities often have cylindrical symmetry and because truly three-dimensional electromagnetic field programs do not exist.

The presentation is further limited to fields which also are rotationally symmetric, i.e. which do not depend on the azimuthal angle θ. It is known from waveguide theory that all such fields are a superposition of two kinds of fields:

i) TM fields (or E fields) with non-zero components, E_z, E_r, H_θ;

ii) TE fields (or H fields) with non-zero components, H_z, H_r, E_θ.

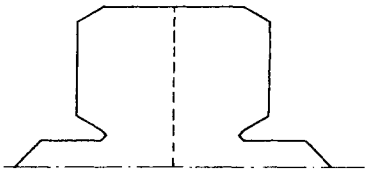

Fig. 2.1 Outline of a cylindrical LEP RF cavity showing nose cones and tapered tubes for closing off the beam tube. The dashed line is a symmetry plane.

Since we are interested in accelerating fields, we limit the presentation to the TM fields with rotational symmetry. This simplifies the task considerably since both the boundary and the fields have no θ dependence. A boundary condition satisfied for one value of θ is automatically satisfied for all values of θ. Essentially, the three-dimensional problem has been reduced to a two-dimensional one.

Proceeding in this manner we miss the theory and computer programs for electromagnetic fields with an azimuthal dependence exp (i mθ), with m $\geq$ 1. Deflecting fields with m = 1 are relevant to accelerator physics. They are excited in RF particle separators in order to separate $\bar{p}$, π^-, and K^- in high-energy particle beams after momentum analysis. Deflecting fields also are responsible for the transverse turbulence observed in e^+e^- storage rings. In general, deflecting fields are a superposition of TE and TM fields in order to satisfy the boundary conditions.

A third approach to electromagnetic field computations shall be mentioned briefly. In programs such as BCI [22] and TBCI [23], the time-dependent Maxwell equations are solved directly in the presence of moving charges by a finite-element technique. This immediately yields the wake potential for a bunch with short but finite length.

2.1 Modes in a disk-loaded waveguide

We want to study electromagnetic fields in a periodic structure with period d and infinite length as shown in Fig. 2.2. We look for circular frequencies ω at which travelling waves propagate with phase velocity v = βc, i.e. in synchronism with particles travelling at speed v.

This problem arises in the design of electron linacs such as the SLAC linac, where waveguide dimensions have to be found such that wave propagation at v = βc occurs at the fixed frequency $\omega = 2\pi \times 2856$ MHz. A similar problem arises in e^+e^- storage rings. The frequency and coupling impedance must be found for many modes, to be used in beam-loading and wake-field calculations.

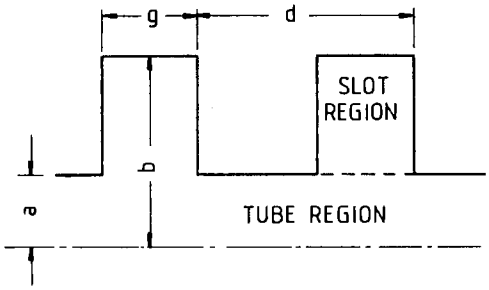

Fig. 2.2 Shape of the periodic RF cavities handled by the KN7C program. The fields in the tube and slot regions are matched across the dashed line.

2.1.1 Tube fields

A suitable guess at a solution for the electric field parallel to the cylinder axis in the tube region r $\leq$ a is

$$\varepsilon_z(r,z,t) = E_z(r,z) \exp(i\,\omega t) \,. \tag{2.2}$$

Since the boundary conditions are periodic, the spatial part $E_z(r,z)$ can be written in the following form:

$$E_z(r,z) = e_z(r,z) \exp(-i\,\beta_0 z) \,. \tag{2.3}$$

Here $\beta_0 = \omega/v - 2\pi\,\ell/d$ is a phase factor with ℓ chosen such that $|\beta_0| < \pi/d$. The function $e_z(r,z)$ is periodic in z and can therefore be expanded into a Fourier series. With $\beta_m = \beta_0 + 2\pi\,m/d$, Eq. (2.3) becomes

$$E_z = \sum_{m=-\infty}^{+\infty} A_m(r) \exp(-i\,\beta_m z) \,. \tag{2.4}$$

The explicit radial dependence $A_m(r)$ follows from the Maxwell equations. It is given by Bessel functions. In the tube region including the origin, $r = 0$, $A_m(r)$ must remain finite. This implies that Eq. (2.4) can be written

$$E_z = \sum_m A_m \left[J_0(\chi_m r)/J_0(\chi_m a)\right] \exp(-i\,\beta_m z) , \tag{2.5}$$

with $\chi_m^2 = (\omega/c)^2 - \beta_m^2$. This formulation invites two comments. When $\chi_m^2 < 0$ the function J_0 should be replaced by I_0, with the appropriate change of argument. Although I_0 grows exponentially with its argument, the ratio $I_0(\chi_m r)/I_0(\chi_m a)$, with $r \leq a$, behaves reasonably for all arguments. At CERN, special routines are available which do not contain multiplications with an exponential [24]. For later use, we record H_θ with $Z_0 = 120\pi\,\Omega$, the impedance of free space:

$$Z_0 H_\theta = (i\,\omega/c) \sum_m A_m \left[J_1(\chi_m r)/\chi_m J_0(\chi_m a)\right] \exp(-i\,\beta_m z) . \tag{2.6}$$

The coefficients A_m in Eqs. (2.5) and (2.6) will be determined later.

2.1.2 Slot fields

In the slot region with $r \geq a$ and $|z| \leq {}^1/_2\,g$, a suitable guess should satisfy the boundary conditions $E_z = 0$ for $r = b$, and $E_r = 0$ for $|z| = {}^1/_2\,g$. This is achieved with standing waves:

$$E_z = \sum_{s=0}^{\infty} B_s \cos(2\pi\,sz/g) \left[F_0(\Gamma_s r)/F_0(\Gamma_s a)\right] + \sum_{s=1}^{\infty} D_s \sin\left[(2s-1)\,\pi z/g\right] \left[F_0(\Gamma'_s r)/F_0(\Gamma'_s a)\right] , \tag{2.7}$$

$$Z_0 H_\theta = (i\,\omega/c) \sum_s B_s \cos(2\pi\,sz/g) \left[F_1(\Gamma_s r)/F_0(\Gamma_s a)\right] + (i\,\omega/c) \sum_s D_s \sin\left[(2s-1)\,\pi z/g\right] \left[F_1(\Gamma'_s r)/F_0(\Gamma'_s a)\right] , \tag{2.8}$$

with the propagation constants

$$\Gamma_s^2 = (\omega/c)^2 - (2\pi\,s/g)^2, \quad \Gamma_s'^2 = (\omega/c)^2 - \left[(2s-1)\,\pi/g\right]^2 , \tag{2.9}$$

and the functions

$$F_i(\Gamma r) = Y_0(\Gamma b)\,J_i(\Gamma r) - J_0(\Gamma b)\,Y_i(\Gamma r) , \tag{2.10}$$

with the obvious property $F_0(\Gamma b) = 0$. The coefficients B_s and D_s remain to be determined. Splitting the slot fields into odd and even ones as done above, is not necessary. It has the advantage of cutting the length of the sums by a factor of two.

2.1.3 Field matching

The next step towards a solution of the electromagnetic field is to determine the coefficients A_m, B_s, and D_s. This is done by imposing the last remaining boundary condition along the surface $r = a$. We require firstly that $E_z = 0$ for ${}^1/_2\,g \leq |z| \leq {}^1/_2\,d$, and secondly that the tangential field components be continuous across the slot mouth, i.e. $E_{zt} = E_{zs}$ for $|z| \leq {}^1/_2\,g$, and $H_{\theta t} = E_{\theta s}$ for $|z| \leq {}^1/_2\,g$. The indices s and t refer to

the slot fields [Eqs. (2.7) and (2.8)] and the tube fields [Eqs. (2.5) and (2.6)], respectively. Writing the boundary conditions explicitly leaves us with rather messy equations:

$$\sum_m A_m \exp(-i\,\beta_m z) = \begin{cases} 0 & \text{for } \tfrac{1}{2} g \le |z| \le \tfrac{1}{2} d \\ \sum_s B_s \cos(2\pi\, sz/g) + \sum_s D_s \sin\left[(2s-1)\,\pi\, z/g\right] & \text{for } |z| \le \tfrac{1}{2} g \end{cases} \tag{2.11}$$

$$\sum_m \frac{d}{g} A_m M_{mm} \exp(-i\,\beta_m z) = \sum_s B_s \cos(2\pi\, sz/g)/H_{ss} + \sum_s D_s \sin\left[(2s-1)\,\pi\, z/g\right]/L_{ss} \,. \tag{2.12}$$

Here the following abbreviations were introduced, with the Kronecker symbol δ_{0s}:

$$\begin{aligned} H_{ss} &= (1+\delta_{0s})\Gamma_s F_0(\Gamma_s b)/F_1(\Gamma_s b) \\ L_{ss} &= 2\Gamma'_s F_0(\Gamma'_s b)/F_1(\Gamma'_s b) \\ M_{mm} &= J_1(\chi_m a)\, g/d\, \chi_m J_0(\chi_m a) \,. \end{aligned} \tag{2.13}$$

The coefficients A_m, B_s, and D_s can be isolated by using the orthogonality of the exponential and trigonometric functions. Equation (2.11) is multiplied by $\exp(+i\,\beta_n z)$ and integrated from $-\frac{1}{2}d$ to $+\frac{1}{2}d$, and becomes

$$A_n = \sum \frac{g}{d} B_s \int_{-\frac{1}{2}g}^{+\frac{1}{2}g} g^{-1} \cos(2\pi\, sz/g) \exp(+i\,\beta_n z)\, dz \,, \tag{2.14}$$

$$+ \sum_s \frac{g}{d} D_s \int_{-\frac{1}{2}g}^{-\frac{1}{2}g} g^{-1} \sin\left[(2s-1)\,\pi\, z/g\right] \exp(+i\,\beta_n z)\, dz \,. \tag{2.15}$$

Similarly, B_t and D_t are isolated by multiplying Eq. (2.12) with $\cos(2\pi\, tz/g)$ and $\sin[(2t-1)\pi z/g]$, and integrating from $-\frac{1}{2}g$ to $+\frac{1}{2}g$:

$$B_t = \sum_m \frac{d}{g} A_m M_{mm} H_{tt} \int_{-\frac{1}{2}g}^{g/2} g^{-1} \cos(2\pi\, tz/g) \exp(-i\,\beta_m z)\, dz \,,$$

$$D_t = \sum_m \frac{d}{g} A_m M_{mm} L_{tt} \int_{-g/2}^{g/2} g^{-1} \sin\left[(2s-1)\,\pi\, z/g\right] \exp(-i\,\beta_m z)\, dz \,. \tag{2.16}$$

2.1.4 Matrix formulation

The notation can be greatly simplified by realizing that the previous equations lend themselves to matrix-and-vector notation:

$$\begin{aligned} A &= \left[C^T B + S^T D\right] g/d \,, \\ B &= \left[HCMA\right] d/g \,, \\ D &= \left[LSMA\right] d/g \,. \end{aligned} \tag{2.17}$$

Here C and S are the integrals in Eqs. (2.15) and (2.16), the index T indicates a transposed matrix, and H, L, M are diagonal matrices. By eliminating B and D, a homogeneous equation for A is obtained, with the unit matrix U:

$$\left[C^{T}HCM - S^{T}LSM - U\right] A = 0 \ . \tag{2.18}$$

The frequencies ω, where Eq. (2.18) has non-trivial solutions, are the frequencies where modes with phase velocity βc propagate through the periodic structure.

The physical problem of finding these frequencies has thus been reduced to a numerical one: finding the zeros of the determinant of an infinite matrix, and solving a homogeneous system of equations. This is a standard problem in numerical analysis. Most computer systems have efficient routines for solving it.

2.1.5 Pitfalls

For practical reasons the infinite matrices are truncated. A safe criterion for the upper limits $\hat{s}$ and $\hat{m}$ for the indices s and m is that half a wavelength at the maximum frequency ω_{max} is about equal to $d/\hat{m}$. This implies $\hat{m} = d\,\omega_{max}/\pi c$. Since the time necessary to compute a determinant for a matrix of order $2\hat{m}$ is proportional to $\hat{m}^3$, there is a practical upper limit for ω. This is further aggravated by the fact that the density of modes in a given frequency interval increases linearly with ω in the asymptotic limit $\omega \to \infty$.

The determinant of the matrix in formula (2.18) has infinities at all frequencies where any element of H, L, or M tends towards infinity, i.e. at the zeros of their denominators. In order not to confuse the zero-finding routine with these infinities, it is best to compute them in advance and to multiply Eq. (2.18) with them. The modified determinant is finite in the whole frequency interval considered and has the same zeros as the original determinant.

Stepping through a frequency interval in regular steps does not guarantee that all zeros are actually found. On the contrary, zeros which occur in pairs within a single frequency step will certainly not be found. In order to find those, one may list or plot another modified determinant from which also the known zeros have been divided out. This function has sharp dips in the neighbourhood of the missing zeros. They can be found by stepping through these regions with smaller frequency steps.

2.1.6 Solution

Any multiple of a solution of a homogeneous system of linear equations is also a solution. This arbitrary scale factor can be determined from the requirement that the vector potential be normalized as follows, with V the volume of one cell and ε_0 the permittivity of free space:

$$\varepsilon_0 \int_V \left|\underline{A}\ (\underline{r})\right|^2 \mathrm{d}V = 1 \ . \tag{2.19}$$

When this condition is satisfied, the relation between the coefficients A_m and the higher-order loss parameter k for one particular mode becomes simply

$$k = \tfrac{1}{2}(A_\ell d)^2 \ . \tag{2.20}$$

Here ℓ is chosen such that $\beta_\ell = \omega/v$. The loss parameter describes the average energy loss of the particles in a bunch when it passes through one period. For a bunch with charge q, the retarding voltage is $V = kq$, and the energy loss is $W = kq^2$. By energy conservation, this energy is stored in a particular mode after the passage of the bunch.

The calculations described are contained in the KN7C [25] code. Its equivalent for deflecting modes is called TRNSVRSE [26]. Both programs work for cavities with a shape as schematically shown in Fig. 2.2. For this geometry they are much faster than other programs. As an example, Fig. 2.3 shows the results [27] for a LEP RF cavity in the form of a histogram of loss factors which have been grouped into bins of 250 MHz width.

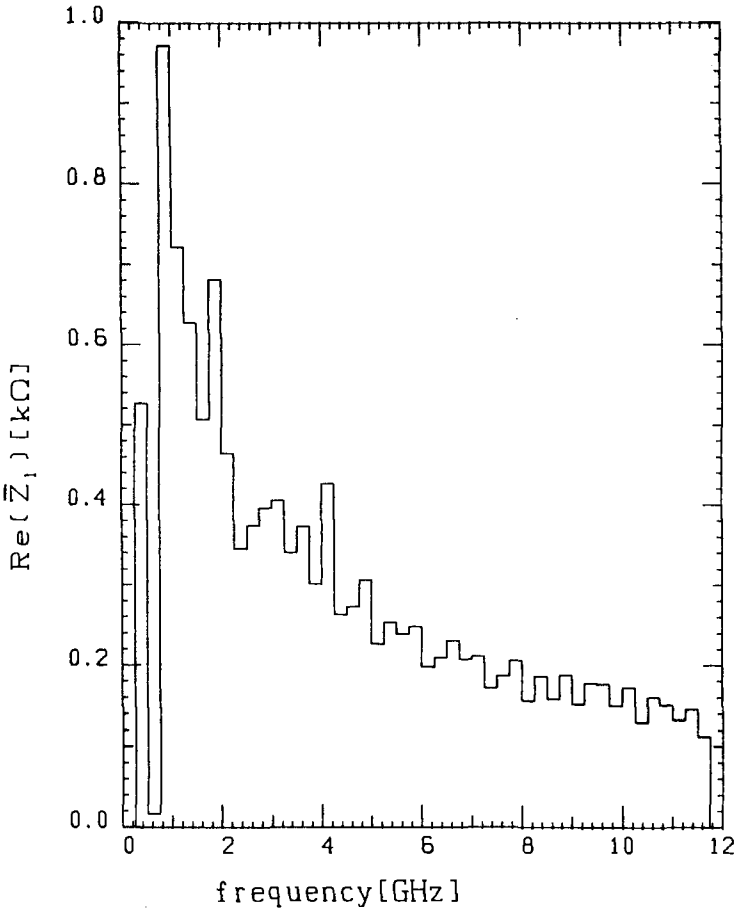

Fig. 2.3 Histogram of the broad-band impedance for an RF cavity in LEP obtained with the KN7C program (from Ref. 27).

2.1.7 Summary for field matching

The field matching technique works best for cavities with a simple shape which can be divided into even simpler regions such that the solution in these regions can be guessed. There should not be too many boundaries between regions across which the tangential field components must be matched.

2.2 Resonant frequencies and shunt impedance of RF cavities

Realistic RF cavities for e^+e^- storage rings have a more complicated shape than that shown in Fig. 2.2, even when perturbations to the cylindrical geometry due to tuners, couplers, etc., are not considered. Since the cavity walls are no longer surfaces parallel to the coordinate axes, the simple technique of field matching can no longer be applied, and purely numerical techniques have to be used.

Several of the steps taken to obtain a solution for the resonant frequencies and the shunt impedances associated with them will be discussed below as they are used in the SUPERFISH [28] program.

The following assumptions are made

i) The cavity has cylindrical geometry and is closed, as shown in Fig. 2.1. Since realistic cavities have beam holes, these holes must be replaced by the tape red tubes shown. The perturbation thus introduced must be investigated.

ii) The magnetic field is proportional to cos ωt, whilst the electric field is proportional to sin ωt. This follows from the Maxwell equations and is no restriction of generality.

iii) The electromagnetic field is independent of the azimuthal angle θ.

iv) The parallel component of the electric field vanishes on all surfaces, assumed to be perfectly conducting. The magnetic field vanishes along the cylinder axis $r = 0$, and possibly on selected surfaces as shown in

Fig. 2.1. Exploiting the symmetry of the cavity and of the modes in this manner will halve the problem.

When the time dependence is divided out and the units for E and H are chosen appropriately, the Maxwell equations can be written with the wave numbers $k = \omega/c$:

$$\nabla \times \underline{H} = k\underline{E} \ ,$$
$$\nabla \times \underline{E} = k\underline{H} \ . \qquad (2.21)$$

The objective is to find values of k for which Eqs. (2.21) are satisfied. It is reached in a number of steps.

2.2.1 The mesh

The SUPERFISH program uses an irregular triangular mesh, whilst other programs use rectangular or quadratic meshes. The first step is to define a logical mesh, using a sheet of paper covered with equilateral triangles. The mesh points are identified by labels K along the cylinder axis, and labels L in the radial direction. A topological outline of the RF cavity is also drawn into the logical mesh, as shown in Fig. 2.4. In this way, the relation between important points of the cavity, e.g. corners, and the logical mesh is established.

This correspondence between logical mesh points and coordinates of the cavity outline is fed into an automatic mesh generator. It distorts the logical mesh such that all cavity boundaries fall on mesh lines. This physical mesh is topologically identical to the logical one. The (r,z) coordinates of all points, both boundary and interior points, can be calculated. The physical mesh thus obtained from the logical mesh is shown in Fig. 2.5.

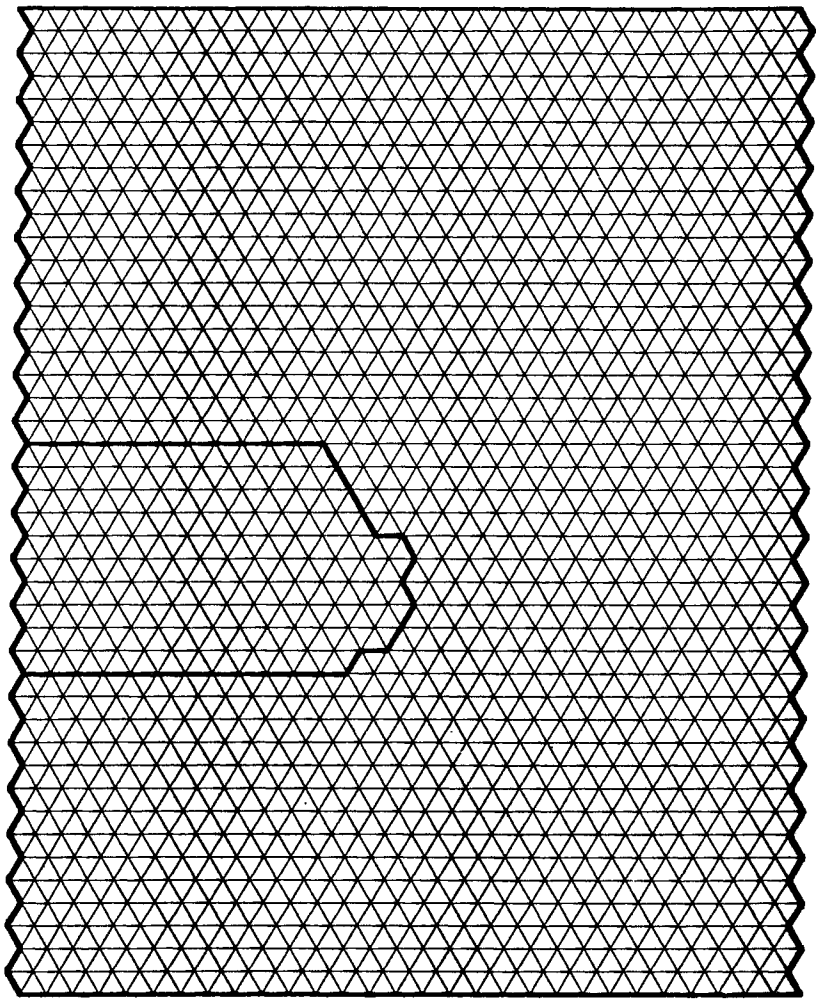

Fig. 2.4 Logical mesh for half a PEP cavity (from Ref. 43).

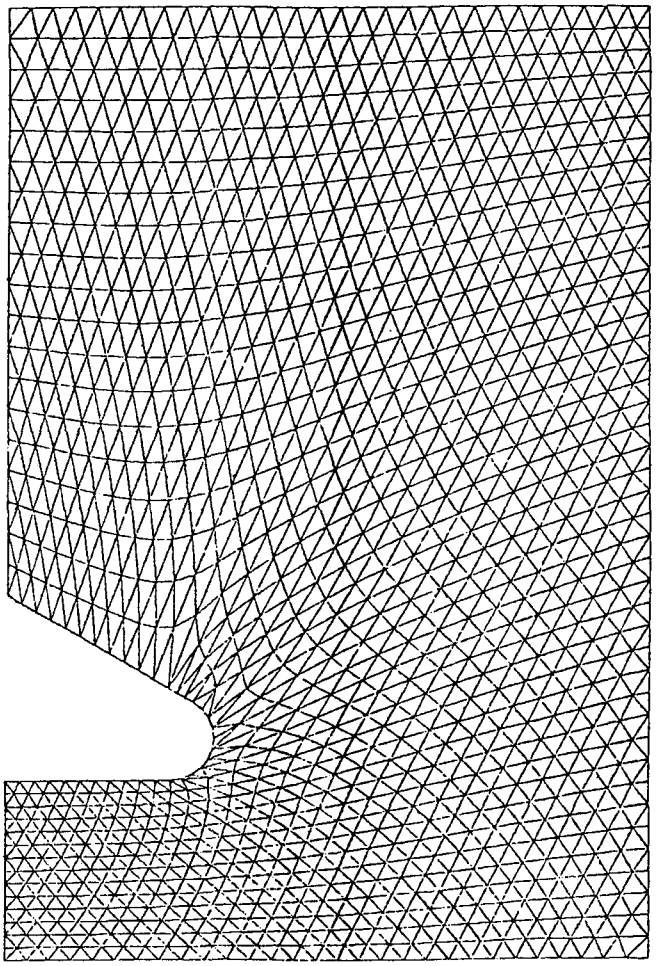

Fig. 2.5 Physical mesh for half a PEP cavity (from Ref. 43).

2.2.2 Difference equations

Eliminating $\underline{E}$ from Eq. (2.21) yields

$$\nabla \times (\nabla \times \underline{H}) = k^2 \underline{H} \ . \tag{2.22}$$

Using a standard formula of vector calculus, this may be expressed as follows:

$$\int \nabla \times (\nabla \times \underline{H}) \cdot d\underline{a} = \oint \nabla \times \underline{H} \, ds = k^2 \int \underline{H} \cdot d\underline{a} \ . \tag{2.23}$$

The only non-vanishing component of $\underline{H}$ is H_ϕ, which SUPERFISH uses to describe the electromagnetic field. Consider now the numerical solution of Eq. (2.23) in the neighbourhood of an interior mesh point, labelled 0 in Fig. 2.6.

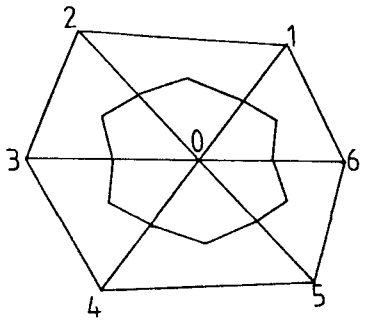

Fig. 2.6 Mesh point surrounded by six triangles and secondary dodecagon.

The central mesh point is surrounded by six triangles. A secondary dodecagon is constructed by joining the centres of the mesh lines radiating from the central mesh point, and the centres of gravity of the six triangles. Assuming that H_ϕ is a linear function of r and z inside each triangle, H_ϕ is uniquely determined everywhere in that triangle by its values at the corners. Hence, Eq. (2.23) can be written in the form:

$$\sum_{n=0}^{6} H_n \, (V_n + k^2 W_n) = 0 \, . \tag{2.24}$$

There is one such equation for each interior mesh point; the coefficients V_n and W_n depend only on the mesh-point coordinates (r,z). It is important for the later solution of the system of equations (2.24) that each equation only involves the field along a mesh line and its two neighbouring mesh lines.

Points along the cavity boundary and points outside the cavity but inside the logical mesh need a special treatment [28]. It is important that this treatment does not destroy the structure of the equations (2.24).

2.2.3 Solution by block elimination

Writing down the difference equations (2.24) for all mesh points, including boundary and exterior points, results in a system of linear equations of order KL, where now K and L are the maximum values of the mesh-point labels:

$$\begin{bmatrix} a_{11} & a_{12} & & & & & \\ a_{21} & a_{22} & a_{23} & & & & \\ & a_{32} & a_{33} & a_{34} & & & \\ & & \ddots & \ddots & \ddots & & \\ & & & a_{L-1,L-2} & a_{L-1,L-1} & a_{L-1,L} & \\ & & & & a_{L,L-1} & a_{L,L} \end{bmatrix} \begin{bmatrix} \underline{H}_1 \\ \underline{H}_2 \\ \underline{H}_3 \\ \vdots \\ \underline{H}_{L-1} \\ \underline{H}_L \end{bmatrix} = \begin{bmatrix} \underline{G}_1 \\ \underline{G}_2 \\ \underline{G}_3 \\ \vdots \\ \underline{G}_{L-1} \\ \underline{G}_L \end{bmatrix} \tag{2.25}$$

The order of elements is arranged such that $\underline{H}_l$ is a column vector with components H_{kl} (k = 1, ..., K). The right-hand sides $\underline{G}_l$ are arranged in a similar manner. Hence the elements a_{kl} are matrices of order K. Because of the form of the difference equations, the matrices a_{kl} are sparse matrices with very few non-vanishing elements.

The system of equations has a block structure with only one block to the left of the main diagonal block. This suggests the following direct procedure of solution, an extension of the Gauss elimination process to block matrices.

The aim of the elimination process is a system of equations with unit matrices U along the main diagonal, and nothing below the diagonal:

$$\begin{bmatrix} U & b_{12} & & & \\ & U & b_{23} & & \\ & & \ddots & \ddots & \\ & & & U & b_{L-1,L} \\ & & & & U \end{bmatrix} \begin{bmatrix} \underline{H}'_1 \\ \underline{H}'_2 \\ \vdots \\ \underline{H}'_{L-1} \\ \underline{H}'_L \end{bmatrix} = \begin{bmatrix} \underline{G}'_1 \\ \underline{G}'_2 \\ \vdots \\ \underline{G}'_{L-1} \\ \underline{G}'_L \end{bmatrix} \tag{2.26}$$

Here the b_{kl} are matrices of order K resulting from the elimination process, and $\underline{H}'_l$ $\underline{G}'_l$ are the modified field components and right-hand sides. Starting with the last row, the system (2.26) can be solved for $\underline{H}'_L$. Using the result $\underline{H}'_L$ in the last but one row yields the solution for $\underline{H}'_{L-1}$. This procedure is continued until also $\underline{H}'_1$ is determined.

The following procedure will bring the system (2.25) into the form (2.26):

i) Multiply the first row by a_{11}^{-1} and obtain:

$$U \qquad a_{11}^{-1}\, a_{12} \qquad\qquad a_{11}^{-1}\, \underline{H}_1 \qquad a_{11}^{-1}\, \underline{G}_1$$

ii) Subtract a_{21} times this first row from the second row and obtain:

$$0 \qquad a_{22} - a_{21}\, a_{11}^{-1}\, a_{12} \qquad \underline{H}_2 - a_{21}\, a_{11}^{-1}\, \underline{H}_1 \qquad \underline{G}_2 - a_{21}\, a_{11}^{-1}\, \underline{G}_1$$

iii) Obtain U in the second row by applying step (i) to it.

iv) Eliminate a_{32} by using step (ii) on the third row.

This procedure is continued for all rows. The last step is:

...) Multiply the last row by the inverse of the modified matrix $a_{L,L}$

2.2.4 Determination of resonance frequencies

The form of Eq. (2.24) suggests that the form of Eq. (2.25) could actually be achieved, if there were only interior mesh points. However, it remains unclear how a right-hand side comes about in Eq. (2.25). Specific steps have to be taken in the SUPERFISH program to obtain an equation of the form (2.25) which is non-singular and well behaved.

The points included in the logical mesh but outside the cavity volume have their field H set to zero, and their coupling to other mesh points is removed. Points on the cavity boundary and on symmetry lines are treated in a similar fashion.

The inhomogeneous terms $\underline{G}_l$ on the right-hand side of Eq. (2.25) are obtained by including a driving term. To this end, the field value at a suitably chosen off-axis mesh point, the driving point, is prescribed to be unity, and the equation for that mesh point is effectively removed from the system (2.25). Care has to be taken in this operation in order not to destroy the structure of the system (2.25).

When the system (2.25) thus obtained for arbitrary $k = \omega/c$ is solved, the field value H_d at the driving point, as obtained from the field values at the neighbouring mesh points, is in general different from the prescribed value unity. The difference $H_d - 1$ is a measure of how close a solution is.

Hence the linear equation solver for (2.25) must be surrounded by a procedure which steps through k and finds zeros of $H_d - 1$. The values of k when this happens are related to the wanted resonance frequencies $\omega = ck$. At these frequencies one can calculate the pattern of the electromagnetic field inside the cavity, and compute quantities such as the quality factor Q and the shunt impedance Z.

2.2.5 Practical limitations

The range of frequencies which can be covered with the SUPERFISH program is limited for two reasons.

The number of mesh points is limited both by the memory size and the speed of the computers currently available. This limitation causes a lower limit of the mesh size, relative to the cavity dimensions; and hence a lower limit of the wavelength of the resonant modes of at least two mesh sizes. This limitation could be overcome with more powerful computers.

A more fundamental limitation arises from the requirement that the cavity volume is closed, and from the tape red tubes which terminate the beam holes, shown in Fig. 2.1. This approximation might disturb the shape of the electromagnetic fields for modes which are not trapped in the RF cavity but propagate through the beam holes. Hence, SUPERFISH has so far not been used for frequencies higher than the cut-off frequency of the beam tube. This limitation might be overcome by opening the beam holes and imposing periodic boundary conditions.

2.2.6 Outlook

The discussion of numerical techniques for calculating electromagnetic fields was limited to accelerating fields which are independent of the azimuthal angle θ. Programs also exist for calculating deflecting fields. The program ULTRAFISH [29] uses a triangular mesh like SUPERFISH, whilst the program URMEL [30] uses a square mesh.

3. COMPUTER PROGRAMS FOR SIMULATING BETATRON MOTION

3.1 Reasons for using simulation

In this lecture we want to go beyond the linear betatron motion discussed earlier. In particular, we want to study the effects of some non-linear components which were excluded then, although they are installed in a real machine.

The need for doing so becomes obvious when the behaviour of the betatron functions is calculated for particles with a relative momentum error δ different from zero. The r.m.s. momentum spread σ_e in the beam, arising from quantum excitation and radiation damping, is shown in Eq. (1.9). In order to obtain an adequate quantum lifetime, the height of the RF buchets has to be at least 6 to 7 times σ_e [3]. Hence the betatron motion must be stable for at least a momentum spread corresponding to the bucket height.

The most noticeable phenomenon for particles with $\delta \neq 0$ is the variation of the tunes with δ. Figure 3.1 shows a gap in the tunes in the neighbourhood of $Q_x = 58$ and $Q_y = 66$. This is due to a half-integral stopband with complex tunes, which is driven by the mismatch between the insertions and the regular lattice for $\delta \neq 0$. In the example shown in Fig. 3.1 the number of superperiods is four, hence half-integral stopbands occur in the vicinity of all even tunes.

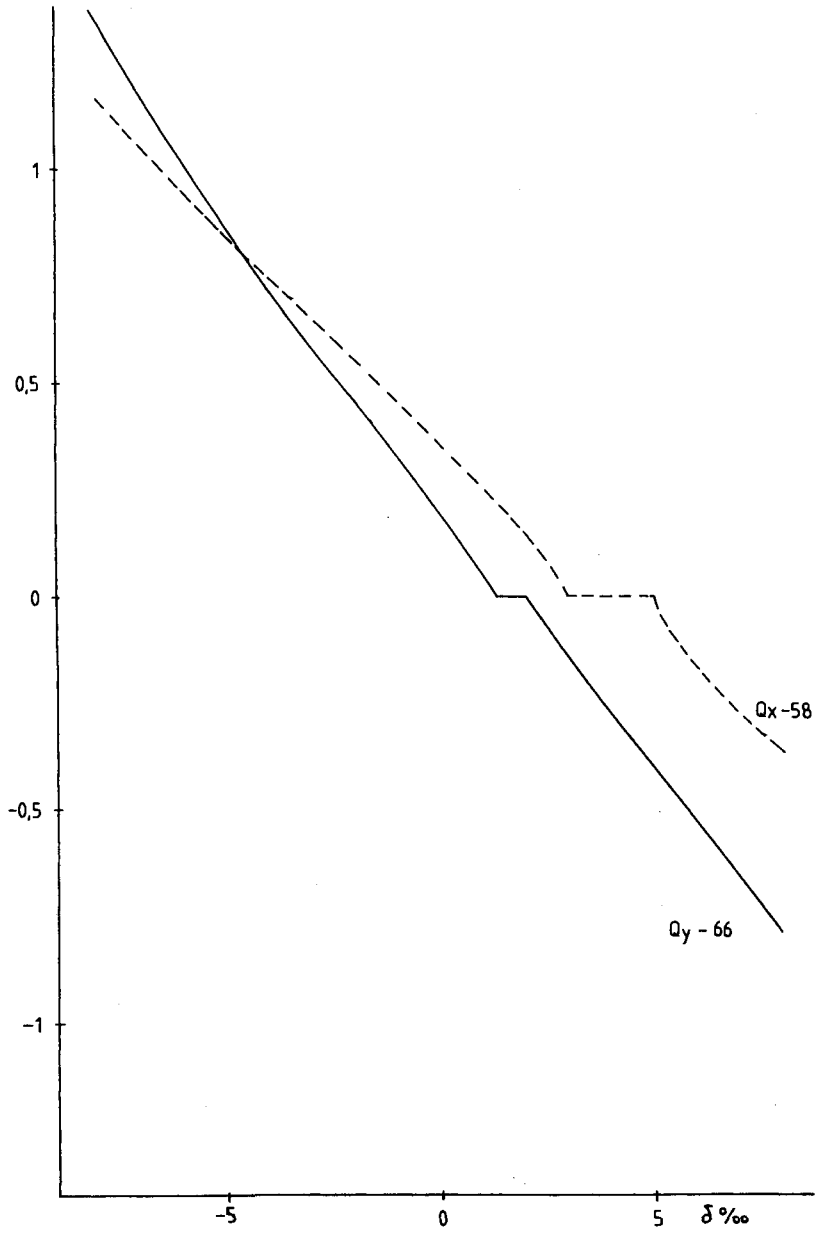

Fig. 3.1 Tune variation with the relative momentum error δ in LEP without chromaticity correction by sextupoles.

The first derivative $Q' = dQ/d\delta$ is called the chromaticity. In a large machine with $Q \gg 1$, contributions to the chromaticity are due to the arcs and to the insertions. The contribution of the arcs, consisting of N_p lattice cells with phase advance μ, is given by

$$Q' = -Q \frac{\tan(\mu/2)}{\mu/2} = -\frac{N_p}{\pi} \tan(\mu/2) \ . \tag{3.1}$$

In Eq. (3.1) Q is the contribution of the arcs to the tune. The contribution of a low-β insertion with amplitude function β at the crossing point and a distance ℓ_x between the crossing point and the nearest quadrupole may be approximated by simply adding the effects of the two nearest quadrupoles on either side of the crossing point:

$$Q' \approx -\frac{\ell_x}{\pi\beta} \ . \tag{3.2}$$

The vertical chromaticity of an insertion is usually larger since β_y is smaller than β_x.

A real machine with errors in the position and excitation of the magnetic elements will have integral stopbands around all integral values of the tunes, and narrower half-integral stopbands around all half-integral tunes. In a machine with a large chromaticity, Q', it is difficult, if not impossible, to avoid all these stopbands by a clever choice of the tunes. In addition, a large negative chromaticity causes a low threshold for the lowest mode of the headtail instability [31]. Therefore the chromaticity must be corrected by sextupoles installed in parts of the machine where the dispersion does not vanish.

By simply arranging the sextupoles in two "families" of equal excitation, e.g. those next to focusing and defocusing quadrupoles, the chromaticities, Q'_x and Q'_y, can be made zero. By having more families, more conditions can be satisfied, e.g. β'_x and β'_y can be made zero at the crossing points. However, sextupoles are non-linear, having cubic terms in the Hamiltonian, and cause undesirable non-linear effects such as

i) systematic third-order resonances;
ii) systematic fourth-order resonances;
iii) higher derivatives, $\partial^n\beta_x/\partial\delta^n$, $\partial^n\beta_y/\partial\delta^n$, $\partial^n Q_x/\partial\delta^n$, and $\partial^n Q_y/\partial\delta^n$, with $n > 1$;
iv) tune shifts with the emittances of the betatron oscillations, $\partial Q_x/\partial E_x$, $\partial Q_y/\partial E_y$, and $\partial Q_y/\partial E_x = \partial Q_x/\partial E_y$;
v) derivatives of the dispersion at the crossing points, $\partial^n D/\partial\delta^n$.

Although considerable thought has been given to chromaticity correction schemes, no such scheme has been found which does not have any of these undesirable side effects of the chromaticity correction by sextupoles. However, individual effects can be suppressed by an appropriate choice of the sextupole arrangement. All schemes in which the sextupoles are arranged in identical pairs, with a phase advance π between the members, do not drive third-order resonances [32]. If the phase advance between members of a pair is π and if the pairs are not interleaved, i.e. if there are no sextupoles belonging to other families between the members of a pair, the tune shifts with emittance also vanish [33].

It is possible to calculate analytically the side effects enumerated above, and this calculation has been incorporated in programs such as HARMON [21]. However, it is difficult to obtain from these calculations the maximum betatron emittances for which the motion is stable. This question is therefore answered by simulating the particle motion on a computer, using tracking programs.

Often, the limits of stable betatron oscillations, the "dynamic acceptance" or "dynamic aperture", are computed after the layout of the linear lattice and the arrangement and excitation of the sextupoles have been fixed. However, it may be more appropriate in the long run to study the connection between the layout of a linear lattice, the arrangement of the sextupoles, and the resulting "dynamic aperture".

3.2 Tracking programs

In a tracking program, the motion of test particles is simulated for a prescribed number of turns in the machine. In electron machines a simulation over a few damping times is usually sufficient, whilst for proton machines considerably longer simulations have been done.

The test particles start with initial conditions which may be combined into a vector $\underline{X}$ of dimension six:

$$\underline{X} = (x, x', y, y', s, \delta) . \tag{3.3}$$

Here, x (y) is the horizontal (vertical) displacement, x′ (y′) is the horizontal (vertical) slope, and s is the accumulated orbit length difference (initially s usually vanishes, it can be neglected in many calculations). Finally, δ is the relative momentum error. In purely magnetic machines δ is constant. The test particles traverse the elements of the machine, i.e. the drift spaces, dipoles, quadrupoles, sextupoles, etc., one by one. In each element, they are transformed according to

$$\underline{X}_f = \underline{T}(\underline{X}_i) . \tag{3.4}$$

Here $\underline{X}_i$ ($\underline{X}_f$) is the vector of initial (final) coordinates and $\underline{T}$ is a vector function. In order to discover anything not already known from the linear lattice programs, $\underline{T}$ must contain terms of higher order than first order in the components of $\underline{X}_i$. Since the final coordinates of the n^{th} element are the initial coordinates for the $(n + 1)^{th}$ element, these transformations may be concatenated:

$$\underline{X}_n = \underline{T}_n \left[\underline{T}_{n-1}\left(\cdots\{\underline{T}_2[\underline{T}_1(\underline{X}_0)]\}\right)\right] . \tag{3.5}$$

Here, $\underline{T}_n$ is the transformation through the n^{th} element. If the concatenation is limited to terms of m^{th} order in $\underline{X}_0$, it can be written as a single transformation:

$$\underline{X}_n = \underline{T}(\underline{X}_0) . \tag{3.6}$$

This is obvious for linear elements with m = 1, for which the $\underline{T}_n$ are the well-known transformation matrices and the concatenation is simply a matrix multiplication. Concatenation up to order m = 2 is incorporated in the TRANSPORT code [12], and terms up to m = 3 in the MARYLIE code [34] based on Lie algebraic techniques.

It should be noted that the formulations (3.5) and (3.6) are identical only up to terms of order m in the components of $\underline{X}_0$. Terms of order > m are absent from (3.6) by definition, whilst they "sneak" into (3.5) by repeatedly applying the transformations $\underline{T}_i$ through the elements. A comparison of tracking results obtained by the two techniques for, say, m = 3 should be made.

If multipole components of order much higher than three are to be included in the tracking, the replacement of a whole string of elements by a single transformation is impossible. For reasons of computer time, tracking through strings of linear elements is done by a single matrix, whilst the non-linear elements are treated individually in several tracking programs, e.g. PATRICIA [18], LILA [35], RACETRACK [36].

Tracking programs need the following input information:

- A description of the elements occurring in the machine and of their sequence. This information is also needed for the optics programs; both kinds of program could use the same input processor.
- A description of the initial conditions of the particle(s) to be tracked.
- Control information for selecting the number of turns and the output, etc.

Tracking programs have the capability of recording the coordinates of all particles at each element and on every turn. Since this is more than can reasonably be digested, the output is best presented in graphical form and even then a selection has to be made. The following displays are among the more useful ones:

- Phase plots of x′ versus x and/or of y′ versus y show m^{th} order resonances because the phase plots approach polygons with m corners, or separate into m islands. There is a choice of plotting one or several particles on a graph. Figure 3.2 was generated by PATRICIA [18] for a single particle. TURTLE [17] can produce two-dimensional histograms for many particles. Figure 3.3 shows the initial distribution, Fig. 3.4 that at the end of one superperiod.
- Fourier analysis of the x and y motion can reveal many resonances. Figure 3.5 shows a rich spectrum obtained when synchrotron motion is included in tracking with PATRICIA.

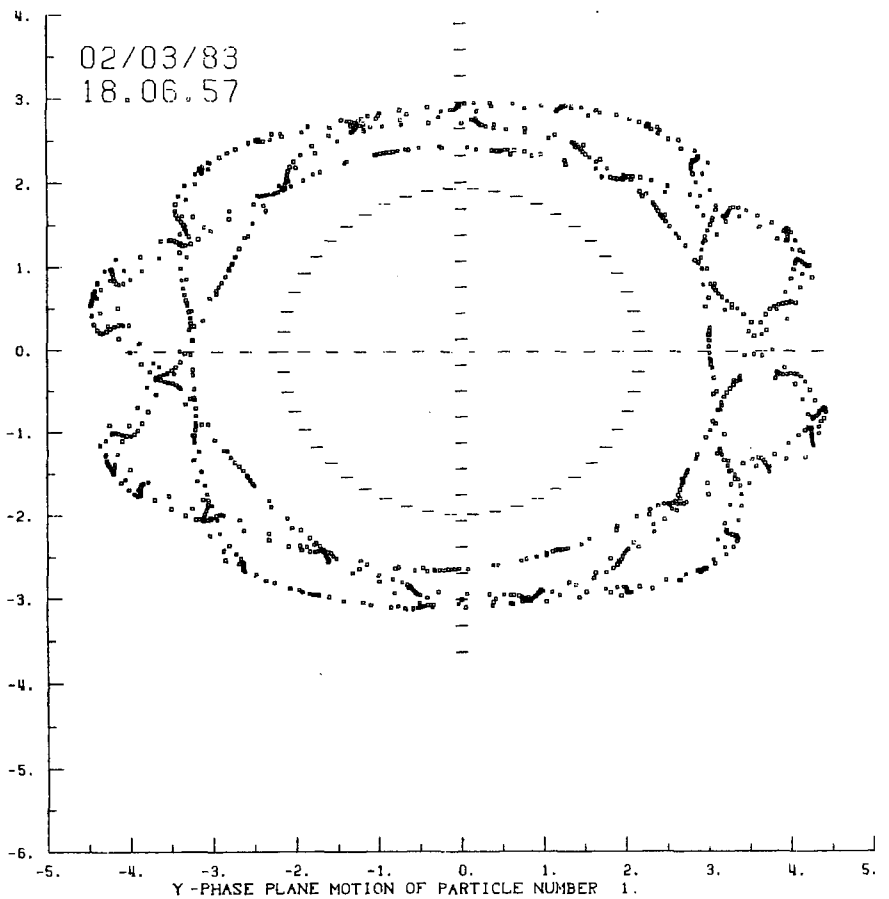

Fig. 3.2 Vertical phase-plane motion of a particle tracked with PATRICIA for 999 turns. The relative momentum error is $\delta = 0.863\%$.

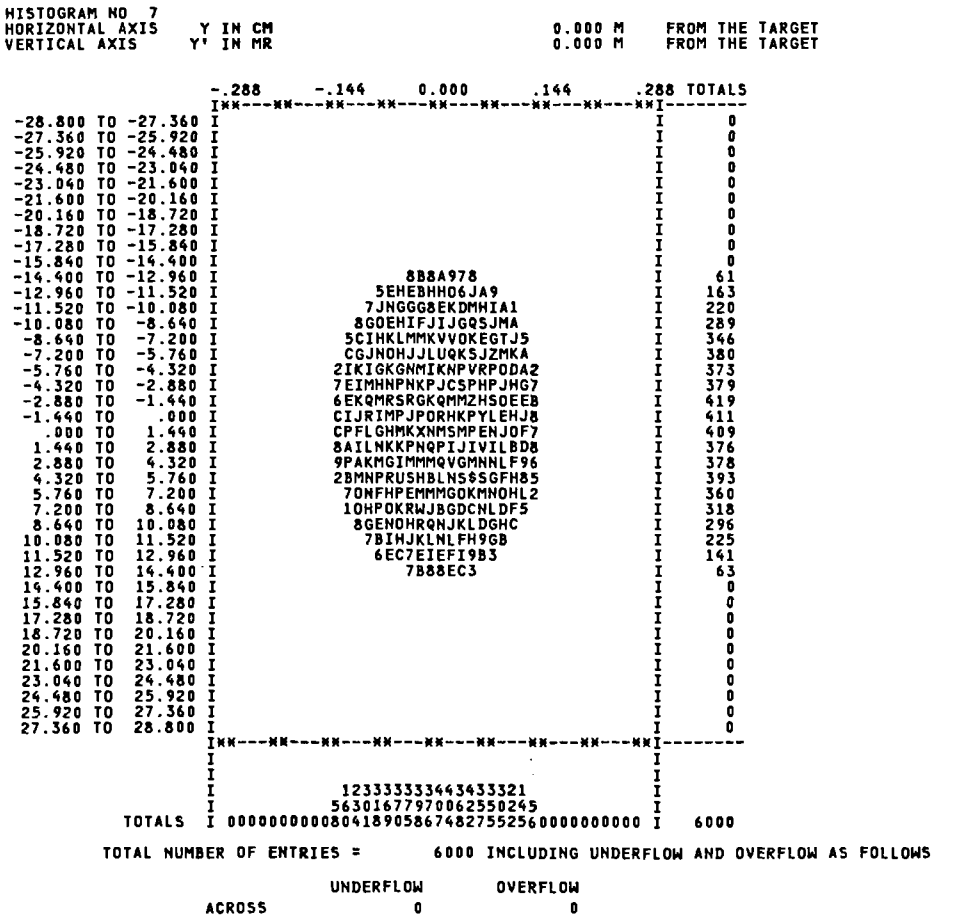

Fig. 3.3 Histogram of the initial vertical phase-plane distribution of 6000 particles to be tracked with TURTLE.

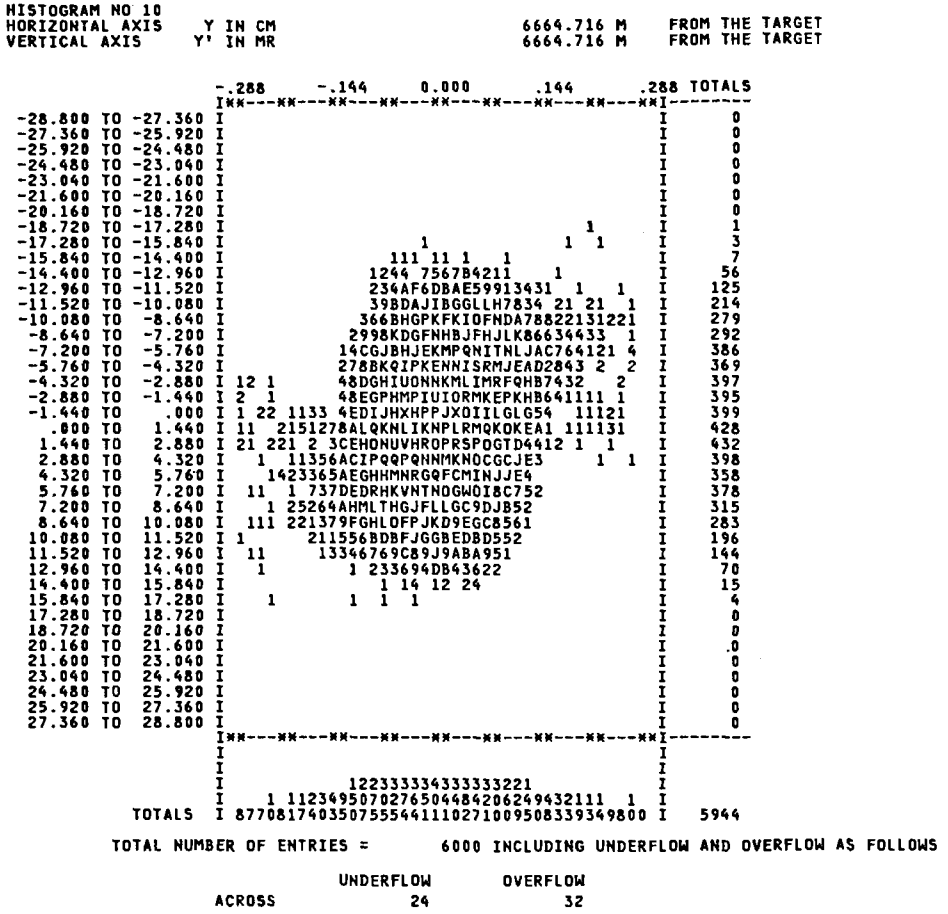

Fig. 3.4 Histogram of the vertical phase-plane distribution of 6000 particles tracked through a superperiod in LEP (6.65 km) with TURTLE.

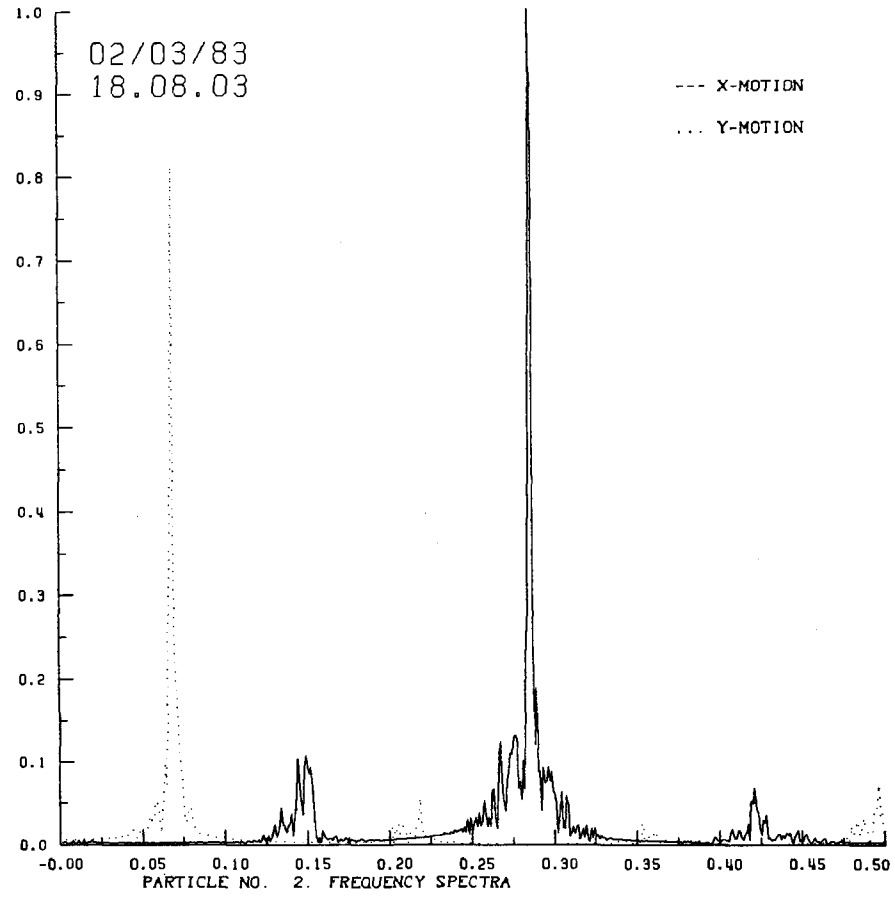

Fig. 3.5 Fourier spectrum of the x and y motion of a particle tracked with PATRICIA for 999 turns. The relative momentum error is $\delta = 0.863\%$.

3.3 Effects due to the momentum error

Putting the momentum error $\delta = 0$ during the tracking allows, in terms of geometrical optics, the study of geometrical aberrations, but excludes the study of chromatic aberrations. In the language of beam optics, effects such as non-linear resonances and tune variations with amplitude, i.e. $\partial Q_x/\partial E_x$, etc., can be studied but chromatic effects such as $\partial^n Q/\partial \delta^n$ and $\partial^n \beta/\partial \delta^n$ cannot. For machines designed to have no geometric aberrations, the tracking results can thus be quite misleading.

Using a non-zero but constant momentum error δ in the tracking program does not make the calculation much more complicated but allows the investigation of chromatic effects. In particular, the maximum permissible value of δ can be found in this way and compared with the value considered necessary for reasons of quantum lifetime (see Section 1).

One may go one step further and vary the momentum error δ with the frequency of synchrotron oscillations Q_s. This allows a study of all the above phenomena and of some coupling effects between betatron and synchrotron oscillations. However, none of the standard tracking programs contain code for a proper simulation of synchrotron-betatron resonances. Varying δ periodically brings the added complication that the transformations must be performed for a range of momentum errors.

In going from vanishing momentum error δ through a constant but non-zero δ to a periodically varying δ, the number of physical effects included in the simulation increases as well. Hence the interpretation of the results becomes more complicated. At the same time, the maximum stable amplitudes of betatron and synchrotron oscillations may decrease. Therefore it is important that the tracking program includes a realistic model of the beam behaviour in a machine.

3.4 Conclusion

The tracking programs presented here are a typical example of solving a problem in single-particle dynamics by computer simulation.

i) The physical ingredients are relatively simple and well known, namely a library of transformations through a small number of element types.
ii) These transformations are chained together in an obvious way given by the sequence of elements in a machine.
iii) The effects to be discovered by the simulation are due to the combined action of the various ingredients.
iv) It is not known *a priori* which effect dominates, and to find this out is one of the purposes of the simulation.
v) If the dominant effect were known from the beginning, more direct analytical approaches might even shed more light.

Putting it very briefly: the purpose of simulation is to obtain some new physics out of a combination of known ingredients.

4. SIMULATION OF BUNCH LENGTHENING

4.1 Motivation

The desire to simulate the motion of electrons (or positrons) in synchrotron phase space arose from the observation in several smaller e^+e^- storage rings that the bunch length and energy spread agreed with the known expressions [3] only at small current. With increasing current both the bunch length and the energy spread increase. This increase is attributed to the interaction between the particles in a bunch and the electromagnetic fields which they excite in the vacuum envelope. For large machines these fields decay between the passages of successive bunches, and the problem can be formulated in terms of the wake field. The objective of the simulation programs to be discussed is a prediction of the bunch length and energy spread for machines which are under construction. However, the only way of checking that these programs contain all the physics necessary to explain the experimental observations is a comparison of their predictions with those observations in existing machines.

4.2 Equations

In a typical simulation program for the longitudinal particle motion, the 10^{11} particles in a typical bunch are represented by a few hundred "superparticles" such that the total bunch charge is correct. The variables in the simulation are ε_i^n, the energy error, and t_i^n, the arrival time at the RF cavity, where i labels the particles and n the turns. For simplicity in the presentation just one RF accelerating system is assumed. The motion of the particles can be described by a pair of recurrence relations between the n^{th} and the $(n+1)^{th}$ turn. The energy equation is:

$$\begin{aligned}\varepsilon_i^{n+1} &= \varepsilon_i^n + eV \sin(\phi + \omega t_i^n) - eU_0 \\ &\quad - \frac{2T_0}{\tau_e}\varepsilon_i^n + 2\sigma_e(T_0/\tau_e)^{\frac{1}{2}} R_i \\ &\quad - e W_i^{n+1} .\end{aligned} \tag{4.1}$$

The first line describes the effect of the RF system (peak voltage V, stable phase angle ϕ, circular frequency ω) and of the synchrotron radiation losses U_0. The second line describes the damping of the synchrotron oscillations (revolution period T_0, damping time τ_e) and of quantum excitation (r.m.s. energy spread σ_e at zero current, uniformly distributed random number $0 \leq R_i \leq 1$). The last line describes the effect of the wake field, i.e. the energy change of the i^{th} particle on the $(n+1)^{th}$ turn W_i^{n+1}. Most of the interesting and difficult aspects of the simulation are hidden in W_i^{n+1}. The time equation is

$$t_i^{n+1} = t_i^n + \frac{\alpha T_0}{E_0}\varepsilon_i^{n+1} . \tag{4.2}$$

Here α is the momentum compaction and E_0 is the energy of the synchronous particle. This equation is a consequence of particles with a higher energy travelling on an orbit further away from the machine centre and therefore taking a longer time.

4.3 Physics of wake fields

During its passage through objects such as RF cavities, the bunch progressively builds up an electromagnetic field in the object, the so-called wake field. This field is superimposed on the fields which might be present due to excitation by an RF transmitter and/or due to previous passages of bunches of the same or of the opposite beam. Since the Maxwell equations are linear, the wake field can be calculated for a cavity which initially has a vanishing field, and added to the field driven externally as implied in (4.1). In the following, it will be assumed that the wake field decays between successive bunch passages.

The wake field is a function of the cavity shape, the coordinates, and the time which may be taken relative to the passage of the bunch centre through the centre of the cavity. Since for relativistic particles with $\gamma \gg 1$ their position relative to the bunch centre is "frozen" during the passage through the cavity, the effect of the wake field can be integrated along the cavity and expressed as a wake potential. This yields a considerable simplification since the wake potential is only a function of the cavity shape, the bunch shape, and of the position (or time) relative to the bunch centre.

There are both longitudinal wake potentials which accelerate the particles, and transverse wake potentials which deflect them. Either of them can be calculated directly using programs such as TBCI [23] which grew out of the BCI program [22] for calculating longitudinal wake fields due to bunches travelling along the axis of cavities with cylindrical geometry. An example of such a wake potential is shown in Fig. 4.1.

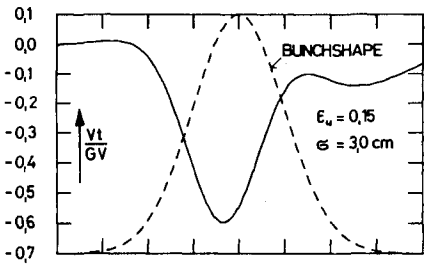

Fig. 4.1 Wake potential of a Gaussian bunch computed by the BCI program (from Ref. 22).

4.4 Use of wake fields in simulations

The discussion in the last subsection points towards a conceptually very simple method for calculating the wake potential in a simulation. It consists of the following simple steps:

- The arrival times t_i^n of the super particles are represented by an appropriate smooth distribution on each turn.
- The wake potential is calculated for this distribution once per turn.
- The wake potential is applied to each super particle.

Although this method is conceptually simple and contains no simplifications, it is unfortunately impractical because the calculation of the wake potential takes too long and dominates the computer time completely. Note, however, that the computer time for applying the wake potential to the superparticles is proportional to their number. In a practical scheme, the full calculation of the wake field once per turn must be avoided. It must be replaced by calculating tables of wake fields once and using the tables once per turn.

A second method of using the wake potential in a simulation is based on the wake potential of point charges, represented by the superparticles. For a given RF cavity geometry, the wake potential w(t) becomes a function of the time t between the particles exciting and observing the wake field. Causality requires that w(t) vanish for $t < 0$. The overall wake field in (4.1) with the total bunch charge Q is then given by,

$$W_i^{n+1} = \frac{Q}{N} \sum_{\substack{j \\ t_i^n > t_j^n}} W(t_i^n - t_j^n) \,. \tag{4.3}$$

The computation of the wake potential w(t) for a point charge is not straightforward. In programs such as BCI, which solve the Maxwell equations with finite space steps Δs and associated time steps $\Delta t = \Delta s/c$, the bunch length must be large compared to Δs, i.e. not a true point charge. This is a fundamental problem called the Courant limit. In addition, there is the practical problem that the memory size required to hold the mesh is proportional to Δs^{-2}, and the computer time is proportional to $\Delta s^{-2}\,\Delta t^{-1}$.

An indirect method of calculating the wake potential of a point charge is based on the fact that the wake potential is the Fourier transform of the cavity impedance. Methods for calculating the latter were given in Section 2, but only up to some finite frequency $\hat{\omega}$. The value of $\hat{\omega}$ is determined by the number of space harmonics carried along in KN7C [25] or by the mesh size in SUPERFISH [28]. Hence, the basic problem cannot be circumvented by solving the Maxwell equations differently. However, an estimate of the impedance at frequencies $> \hat{\omega}$ can be derived from laser theory. Combining the impedances — or loss factors k — from SUPERFISH for the first few modes where the detailed shape of the RF cavity might be important, from KN7C for many more modes, and from the optical resonator model [37] for $\omega \to \infty$, and Fourier transforming it yields the wake potential shown in Fig. 4.2.

Simulations with wake potentials for point charges have been performed at Frascati [38], SLAC [39], and CERN [40]. The bunches were launched with Gaussian density distributions for ε_i and t_i. During the simulation using (4.1) and (4.2), the averages $\langle \varepsilon_i \rangle$ and $\langle t_i \rangle$ and the standard deviations σ_e and σ_t were recorded. The average time $\langle t_i \rangle$ is different from zero because of the higher-order mode losses which change the stable phase angle. The standard deviations σ_e and σ_t are the desired results for bunch widening and bunch lengthening.

In this approach, the computer time is dominated by the application of the wake potential to the superparticles and is proportional to the square of their number N. Simulating with small N introduces noise into the system and causes too large values for σ_e and σ_t. It has been shown that this phenomenon is well described by [40]

$$\sigma_{tN}^2 = \sigma_{t\infty}^2 + A/N \,, \tag{4.4}$$

with a constant A which is physically plausible. Hence (4.4) may be used to extrapolate results obtained with relatively small values of N to the case $N \to \infty$.

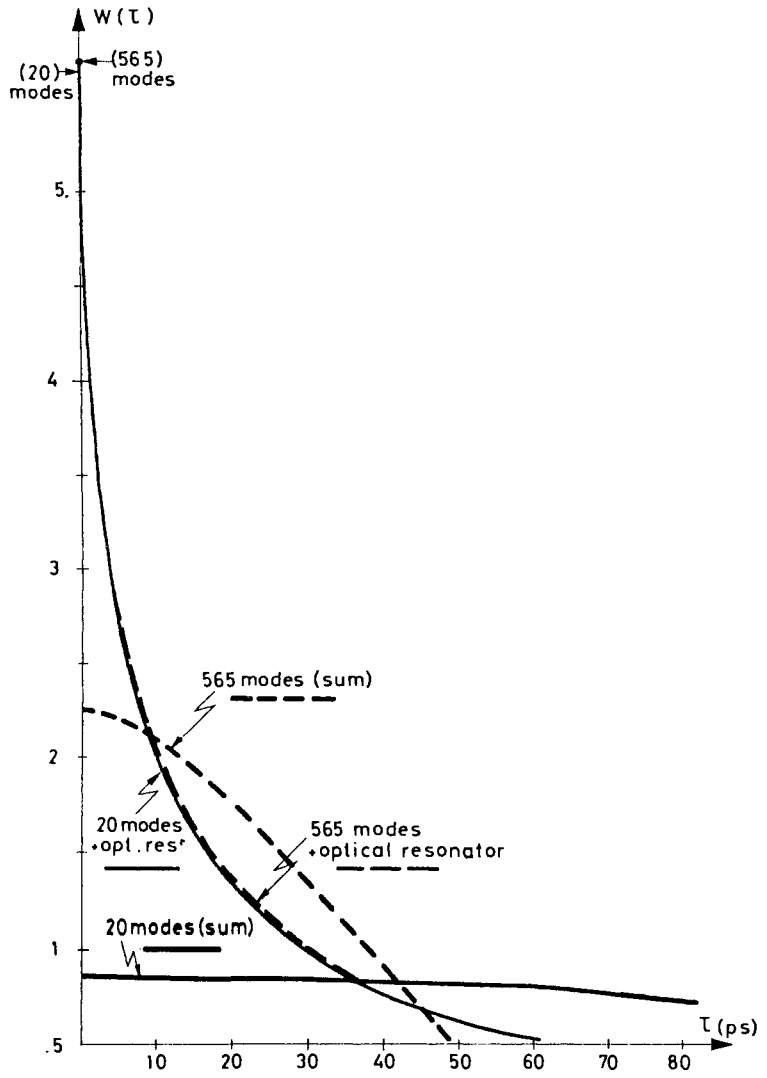

Fig. 4.2 Wake potential for a point charge traversing a LEP RF cavity, using 20 and 565 modes and extrapolation by the optical resonator model (from Ref. 37).

4.5 Binning and fitting

The computer time may be reduced further by replacing the wake potentials for point charges. Two techniques have been used successfully which will be called binning and fitting.

In the first method, binning, the superparticles are put into N_B bins and the same wake is applied to all particles in the same bin. The computer time becomes proportional to N_B. Several variants of this method have been tried:

i) Fixed bins were used in DESY [41]. The wake potential was computed with BCI for a bunch length close to the bin width. The bins in the tail contain few particles while the bins in the core contain many.

ii) Variable bins arranged such that they all contain the same number of particles were used at CERN [40].

iii) A hybrid method was also used at CERN [40]. Here bins were used to describe the wake potential due to particles in earlier bins, but point charges were used for the wakes due to particles in the same bin.

All these methods have given results in good agreement with each other when compared using the same number of superparticles.

In the second method, fitting, a sum of smooth functions is fitted to the density distribution in the bunch. Products of Gaussians and Hermite polynomials are a natural choice for this fit because of the Gaussians present in the orthogonality relation for Hermite polynomials. The computer time is proportional to the product of the number of superparticles and the number of functions in the fit. The wake potential must be computed for all the functions. This method has been used at Cornell [42].

4.6 Conclusions

This second example has shown how a collective phenomenon such as bunch lengthening can be simulated on a computer. Comparing it to the first example, betatron motion, some interesting differences are seen. Firstly, the physics is not simply described by chaining together a series of rather simple operations, i.e. the transformation of coordinates. Secondly, the formulation of the wake potential has a decisive influence on the performance of the simulation code: from the impossible to the reasonable. This performance is achieved by making judicious approximations in the computation of the wake potential.

Simulation is one of the tools used at the forefront of accelerator physics. It helps to identify phenomena which limit the performance of the present generation of e^+e^- storage rings and helps in the design of the next generation. Therefore the largest effort is devoted to the most serious problems.

The two examples given, simulation of the betatron motion in order to define the dynamic acceptance, and simulation of bunch lengthening, are not the only known applications. Simulation is being used now for studying transverse instabilities which are the dominant performance-limiting phenomenon in all larger e^+e^- storage rings, and first results have already been obtained.

The beam-beam interaction is another field to which simulation has been applied for a long time. The recent considerable success teaches us a lesson. In order to simulate a phenomenon well all relevant dynamic processes must be included. Since it is *a priori* not known which processes are relevant, all of them must be included. A full discussion of the beam-beam interaction is given in other lectures at this school.

Acknowledgements

I would like to thank Melvin Month, Gregory Loew and the organizers for a well orchestrated summer school, the staff at SLAC for their hospitality during the school, and finally Ronald Ruth for his help in editing these lectures.

REFERENCES AND FOOTNOTES

[1] E.D. Courant and H.S. Snyder, Ann. Phys. **3,** 1 (1958).
[2] H. Bruck, Accélérateurs circulaires de particules (PUF, Paris, 1966).
[In English: Circular particle accelerators (Los Alamos, LA-TR-72-10 Rev., 1974).]
[3] M. Sands, SLAC-121 (1970).
[4] M.H. Blewett (ed.), CERN 77-13 (1977).
[5] E. Keil, Physics of High Energy Particle Accelerators, AIP Conference Proc. No. 87 (Am. Inst. Physics, New York 1982), p. 805.
[6] B. Richter, Nucl. Instrum. Methods **136,** 47 (1976).
[7] J. Rees and B. Richter, PEP-69 (SPEAR-167) (1973).
[8] R.H. Helm and H. Wiedemann, PEP Note 303 (1979).
[9] Contact E. Keil (CERN) for details about the DESIGN program.
[10] A.S. King, M.J. Lee and W.W. Lee, SLAC-183 (1975).
[11] A.A. Garren and J.W. Eusebio, UCID-10153 (1975).
[12] K.L. Brown, D.C. Carey, Ch. Iselin and F. Rothacker, CERN 80-04 (1980).
[13] E. Keil, Y. Marti, B.W. Montague and A. Sudboe, CERN 75-13 (1975).
[14] F.C. Iselin, private communication (1983).
[15] D.C. Carey, FNAL report TM-1046 (1981).
[16] F. James and M. Roos, CERN Library Program D506 (1967).
[17] K.L. Brown and F.C. Iselin, CERN 74-2 (1974).
[18] H. Wiedemann, PEP Note 220 (1976).
[19] K. Steffen and J. Kewisch, DESY PET 76/09 (1976).
[20] E. Close et al., PEP Note 271 (1978).
[21] M.H.R. Donald, PEP Note 311 (1979).
[22] T. Weiland, Proc. 11th Int. Conf. on High-Energy Accelerators, CERN, Geneva, 1980 (Birkhäuser, Basle, 1980), p. 570.
[23] T. Weiland, DESY 82-015 (1982).
[24] M. Abramowitz and I.A. Stegun, Handbook of Mathematical Functions (Dover, New York 1965), p. 378, and CERN Library Program C313.
[25] E. Keil, Nucl. Instrum. Methods **100,** 419 (1972).
[26] K. Bane and B. Zotter, PEP Note 308 (1979).
[27] K. Bane, CERN/ISR-TH/80-48 (1980).
[28] K. Halbach and R.F. Holsinger, Part. Accel. **7,** 213 (1976).
[29] R.L. Gluckstern et al., Proc. Linear Accelerator Conference, Sante Fe, 1981 (LA-9234-C, Los Alamos National Laboratory, 1981), p. 102.
[30] T. Weiland, DESY M 82-24 (1982).
[31] F. Sacherer, Proc. 8th Int. Conf. on High-Energy Accelerators, Stanford, 1974 (SLAC, Stanford, 1974), p. 347.
[32] L. Di Lella et al., CERN/ISR-AS/74-64 (1974).
[33] K.L. Brown, SLAC-PUB-2257 (1979).
[34] D.R. Douglas and A.I. Dragt, IEEE Trans. Nucl. Sci. **NS-28,** 2522 (1981).
[35] J. Niederer and B. Morris, Proc. Workshop on Accelerator Orbit and Particle Tracking Programs, Brookhaven National Laboratory, May 1982 (BNL-31761, New York, 1982), p. 26.
[36] A. Wrulich, ibid., p. 277.
[37] D. Brandt and B. Zotter, CERN-ISR/TH/82-13 (1982).
[38] A. Renieri, Frascati Report LNF-75/11R (1976).
[39] P.B. Wilson, K.L.F. Bane and K. Satoh, IEEE Trans. Nucl. Sci. **NS-28,** 2525 (1981).
[40] D. Brandt, CERN-ISR-TH/82-09 (1982).
[41] T. Weiland, DESY 81-088 (1981).
[42] R. Siemann, Cornell Report CNLS 82/524 (1982).
[43] R. Early, Users Guide to SUPERFISH, unpublished SLAC report (1977).